Supporting information

In-Situ Anchored Silver Nanoparticles in Porous Organic Polymers for Efficient CO_2 Cyclization with Propargylic Alcohols

Lunbao Chen†, Tao Yang†, Chunliang Yang, Tianxiang Zhao*

Guizhou Provincial Key Laboratory of Green Catalysis and Materials for resource conversion, School of Chemistry and Chemical Engineering, Guizhou University, Guiyang 550025, P. R. China.
E-mail: txzhao3@gzu.edu.cn (T. X. Zhao)
†These authors contributed equally to this work.

Experimental section

Materials

2,4,6-tris(4-aminophenyl)-1,3,5-triazine (APT), 9,10-Phenanthrenequinone 3-methyl-1-pentyn-3-ol, Formaldehyde, DBU, K_2CO_3, $AgNO_3$ and were purchased from Adamas Chemical Co. Ltd. China. Glyoxal, TMG, DBN were purchased from Energy Chemical Co. Ltd. glacial acetic acid (HOAc) were purchased from Titan Scientific Co. Acetonitrile were purchased from Chengdu Jinshan Chemical Reagent Co. Ltd. All chemicals are analytical grade and used directly without any treatment unless otherwise stated. CO_2 (99.99%) and N_2 (99.999%) were purchased from Guiyang Shenjian Gas Center, Guiyang, China.

Characterizations and instruments

N_2 adsorption-desorption isotherms were measured using a BSD-PM2 instrument to analyze pore volume and pore size. All samples were degassed under vacuum at 150 ^oC for 6 h to remove residual air and moisture. The characteristic functional groups and in-situ FTIR spectra (with a CO_2 flow rate was 10 $mL \cdot min^{-1}$) were analyzed using a Nicolet 50 FTIR spectrometer. The microstructures of the materials were characterized by scanning electron microscopy (SEM, ZEISS Gemini SEM 300) and high-resolution transmission electron microscopy (TEM, FEI Talos F200X G2). The crystal structure of the materials was determined using an X-ray diffractometer (D8 Advanced). The thermal stability of the materials was evaluated using a TG 209 F1 Libra thermal analyzer. The carbonate yield was analyzed using a Shimadzu gas chromatograph (GC-2014). The surface properties of the catalyst were investigated via temperature-programmed desorption (TPD). Based on different desorption peaks, acidic or alkaline centers on the catalyst were identified and quantified. Solid-state nuclear magnetic resonance studies (^{13}C CP-MAS NMR, Bruker Avance Neo 400WB, Germany) were employed to obtain the structural information of the materials. Additionally, specific elements were measured and analyzed using inductively coupled plasma (ICP-OES). X-ray photoelectron spectroscopy (XPS, K-Alpha Plus) was utilized to conduct a qualitative analysis of the elemental composition, molecular structure, and valence state of the materials. The Silver (Ag) content was measured using inductively coupled plasma optical emission spectrometry (ICP-OES) on an iCAP PRO instrument.

The synthesis of Ag/POPs

Dissolve 0.9 mmol (approximately 0.319 g) of 2,4,6-tris(4-aminophenyl)-1,3,5-triazine (**APT**) in a bottle containing a mixture of 15 mL of deionized water and 15 mL of acetic acid. Then add 8 mg of

$AgNO_3$ aqueous solution (5 mL) and ultrasonically shake until a uniform suspension solid solution system is obtained. This is the first small bottle. In the second small bottle, add 10 mL of deionized water and 5 mL of acetic acid, mix evenly, and then successively add 5 mmol (0.374 mL) of 37% formaldehyde aqueous solution and 2 mmol (0.42 g) of **1c**, and mix well. Then pour the solutions from the two small bottles into a 100 mL round-bottom flask and reflux in an oil bath at 80 °C for 24 hours. After the reaction is completed, the solid phase obtained is washed with deionized water, DMF, tetrahydrofuran, and acetonitrile (25 mL), centrifuged, and the product is placed in a vacuum oven at 60 °C for vacuum drying for 24 hours, then ground to obtain an orange powder solid.

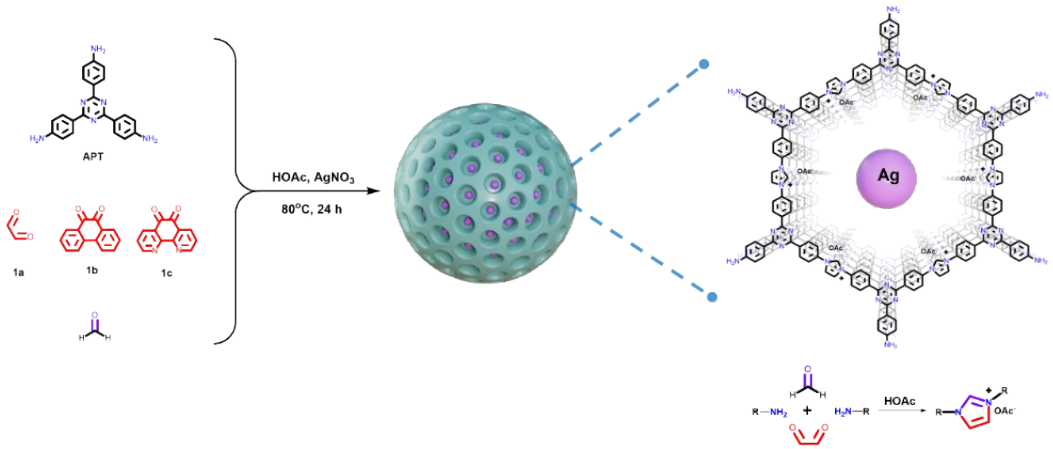

Table S1. Texture properties of the POPs.

Sample	$S_{BET}(m^2 \cdot g^{-1})^a$	$V_{micro}(cm^3 \cdot g^{-1})^b$	$V_{total}(cm^3 \cdot g^{-1})^c$	Average pore sizes (nm)	Ag/ wt%
Ag/POP-1a	39.58	0.003	0.20	26.44	0.065
Ag/POP-1b	179.13	0.008	0.79	18.11	0.071
Ag/POP-1c	102.74	0.0003	0.48	17.47	0.97

[a]BET surface area. [b]Micropore volume. [c]Total pore volume.

Table S2. Comparison of **Ag/POP-1c** with the previously reported heterogeneous catalyst for the cycloaddition of **1a** with CO_2

Entry	Catalyst	*T*(°C)	*p*(bar)	*t*(h)	TON[a]	TOF(h^{-1})[b]	Ref.
1	Ag@UCPP	30	1	24	205	8.5	1
2	Ag MOF-2	25	10	24	133	5.6	2
3	Ag/POP@g-C_3N_4	30	10	12	113	9.5	3
4	Cu/Co_3O_4	120	20	20	111	5.6	4
5	AgF	40	1	6	18	2.9	5
6	Ag(I)@CO_2-Zr-DEDP	30	1	6	33	5.6	6
7	Ag-rGO-3	30	1	12	13	1.1	7
8	1	25	10	10	28	2.8	8
9	Cu_2O@ZIF-8c	50	1	4	12	3.1	9
10	**Ag/POP-1c**	30	1	8	556	70	This work

[a]TON: turnover number was defined as the mole number of product per mole number of catalysts; [b]TOF: turnover frequency was calculated by the mole number of product per mole number of catalysts per hour under the optimal conditions.

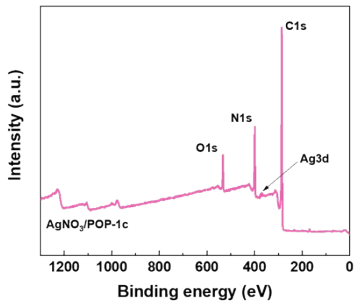

Fig. S1 Survey XPS spectra of **Ag/POP-1c**.

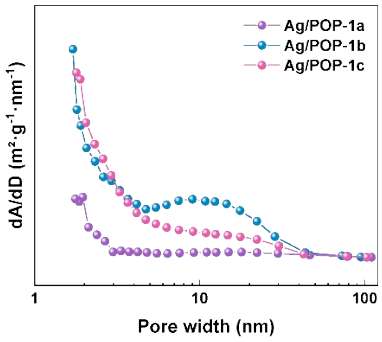

Fig. S2 Pore-size distributions of **Ag/POP**.

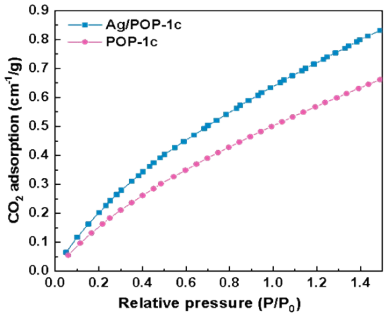

Fig. S3 CO_2 sorption isotherms in **Ag/POP-1c** and **POP-1c** at 298 K.

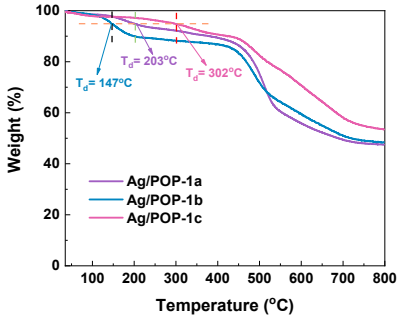

Fig. S4 TGA curves of **Ag/POP-1a**, **Ag/POP-1b**, **Ag/POP-1c**. (The thermal decomposition temperature (T_d) is defined as a mass loss of 5%).

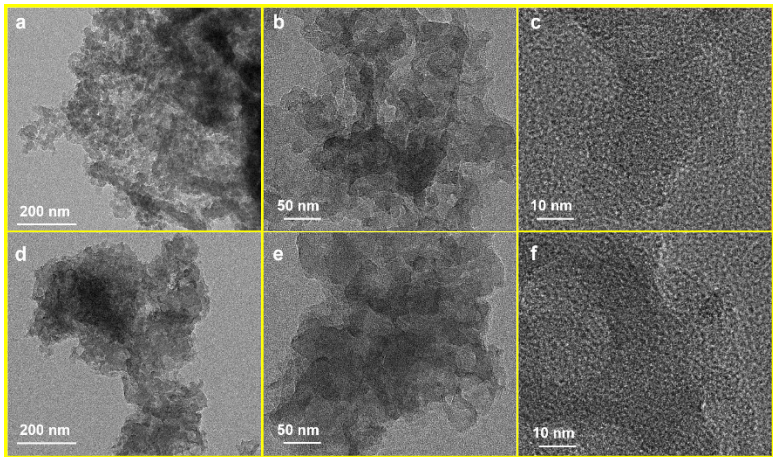

Fig. S5 (a,b) TEM images of **Ag/POP-1a**, (c) HRTEM images of **Ag/POP-1a**, (d,e) TEM images of **Ag/POP-1b**, and (f) HRTEM images of **Ag/POP-1b**.

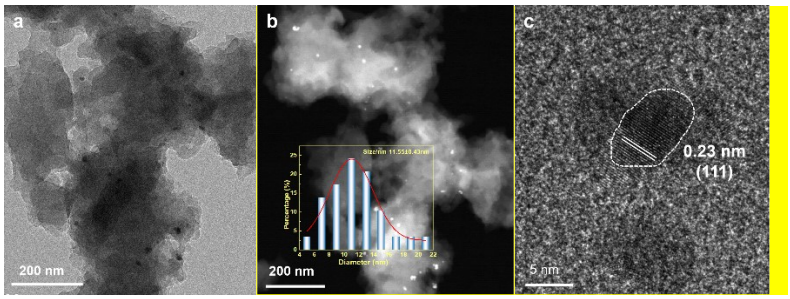

Fig. S6 (a,b) TEM images of after reaction **Ag/POP-1c** (inset: particle size distribution), and (c) HRTEM image of after reaction **Ag/POP-1c**, showing lattice fringes of Ag nanoparticles.

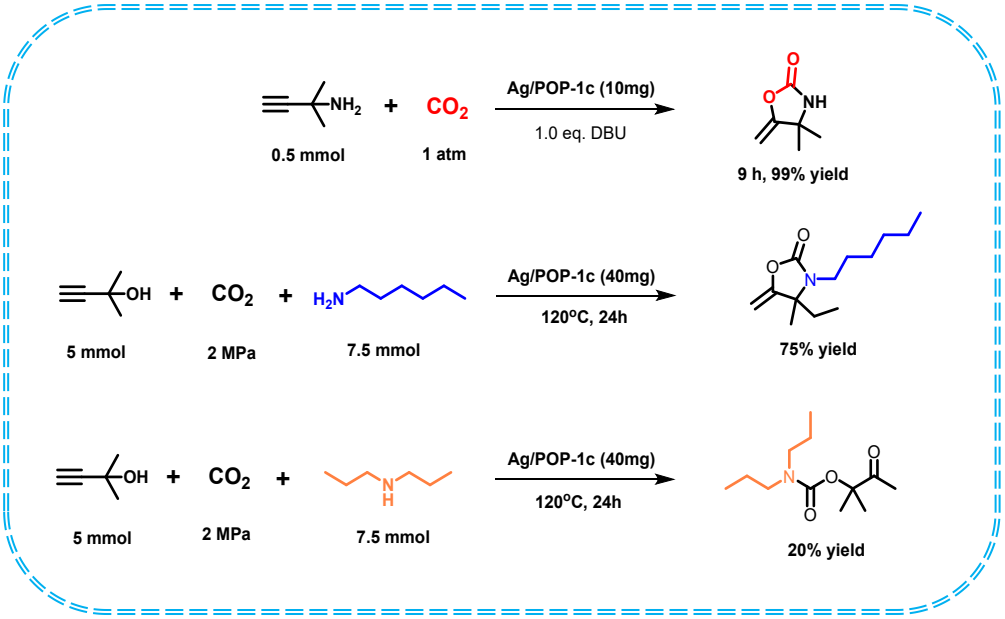

Fig. S7 Yields in three-component reactions with amines

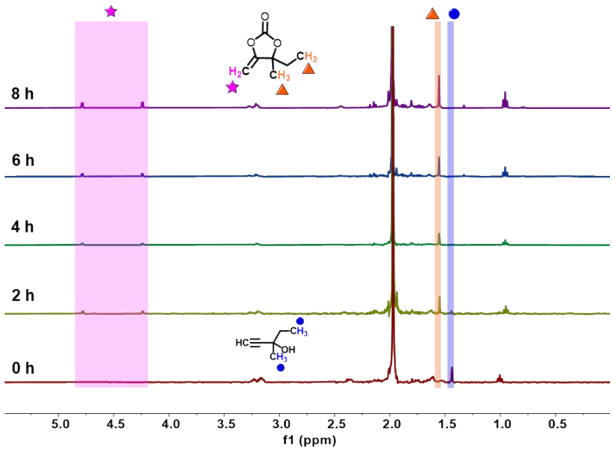

Fig. S8 ^{1}H NMR spectra monitoring the cyclization reaction of 3-methyl-1-pentyn-3-ol with CO_2 catalyzed by **Ag/POP-1c.**

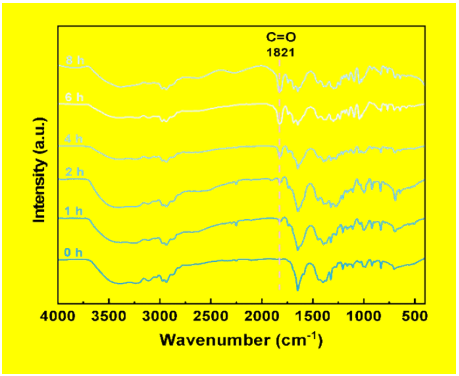

Fig. S9 FTIR spectra of the reaction mixture at different stages.

References

1. X. j. Wang, W. Li, J. X. Wang, J. Zhu, Y. T. Li, X. Z. Liu, L. P. Wang and L. Li, *Dalton Trans.,* 2020, **49**, 13053.
2. Q. Zhang, J. F. Wang, L. Gao, X. Jing and C. Y. Duan, *Chem. Commun.,* 2025, **61**, 9618-9621.
3. C. Du, X. W. Lan, G. Y. An, Q. Li and G. Y. Bai, *ACS Sustainable Chem. Eng.,* 2020, **8**, 7051–7058
4. J. M. Zhou, S. W. Yang, W. H. Wan, L. M. Chen, J. Z. Chen, *J. Catal.,* 2023, **418**, 178-189.
5. X. T. Li, A. V. Yanez, C. N. Tounzoua, J. B. Buchholz, B. Grignard, C. Bo, C. Detrembleur and A. W. Kleij, *ACS Catal.,* 2022, **12**, 2854-2860.
6. B. Song, Y. H. Liang, Y. Zhou, L. Zhang, H. Li, N. X. Zhu, B. Z. Tang, D. Zhao and B. Liu, *J. Am. Chem. Soc.,* 2024, **146**, 14835-14843.
7. X. Zhang, K. H. Chen, Z. H. Zhou and L. N. He, *ChemCatChem,* 2020, **12**, 4825-4830
8. S. Y. Chong, T. T. Wang, H. J. Zhong, L. F. Xu, H. l. Xu, Z. W. Lv and Min. Ji, *Green Energy & Environ.,* 2020, **5**, 154-165.
9. A. L. Gu, Y. X. Zhang, Z. L. Wu, H. Y. Cui, T. D. Hu and B. Zhao, *Angew. Chem. Int. Ed.,* 2022, **61**, e202114817.